

MDPI

Article

Design of Planar Differential Microphone Array Beampatterns with Controllable Mainlobe Beamwidth and Sidelobe Level

Xianghui Wang ^{1,2,*}, Mei Li ^{1,2}, Yingke Zhao ^{1,2}, Jiao Wang ^{1,2} and Xin Tan ^{2,3}

- Center of Intelligent Acoustics and Immersive Communications, School of Electronic Information and Artificial Intelligence, Shaanxi University of Science and Technology, Xi'an 710021, China
- Shaanxi Joint Laboratory of Artificial Intelligence, Shaanxi University of Science and Technology, Xi'an 710021, China
- School of Electronic Information and Artificial Intelligence, Shaanxi University of Science and Technology, Xi'an 710021, China
- * Correspondence: wangxh@sust.edu.cn

Abstract: The differential microphone array, or differential beamformer, has attracted much attention for its frequency-invariant beampattern, high directivity factor and compact size. In this work, the design of differential beamformers with small inter-element spacing planar microphone arrays is concerned. In order to exactly control the main lobe beamwidth and sidelobe level and obtain minimum main lobe beamwidth with a given sidelobe level, we design the desired beampattern by applying the Chebyshev polynomials at first, via exploiting the structure of the frequency-independent beampattern of a theoretical *N*th-order differential beamformer. Next, the so-called null constrained and least square beamformers, which can obtain approximately frequency-invariant beampattern at relatively low frequencies and can be steered to any direction without beampattern distortion, are proposed based on planar microphone arrays to approximate the designed desired beampatterns. Then, for dealing with the white noise amplification at low-frequency bands and beampattern divergence problems at high-frequency bands of the null constrained and least square beamformers, the so-called minimum norm and combined solutions are deduced, which can compromise among the white noise gain, directivity factor and beampattern distortion flexibly. Preliminary simulation results illustrate the properties and advantages of the proposed differential beamformers.

Keywords: microphone array; fixed beamformer; differential beamformer; frequency-invariant beampattern; main lobe beamwidth; sidelobe level



Beamforming based on sensor/antenna array [1–7] has attracted much attention since the apparent advantage over the single sensor/antenna. The earliest beamforming technique is the delay-and-sum (DS) structure, which is investigated widely in narrowband applications [8–11], such as radar, sonar and antenna. However, the drawbacks of the varying beampattern with frequency and low directivity factor (DF) at low-frequency bands make the DS beamformer unsuitable for dealing with broadband signals, such as speech.

To overcome these drawbacks, many broadband beamforming methods have been developed, including the narrowband decomposition methods [12,13], the nested-array framework [14–16], the modal beamforming techniques [17–20], the super directive algorithms [21–23] and the differential beamformers (or differential microphone arrays, DMAs) [24–29]. Among those, the DMAs have been widely studied as they exhibit frequency-invariant beampatterns and high DF. Moreover, they are usually small and compact in size and consequently can be easily integrated into small devices, such as hearing aids, smartphones, smart wearable devices, etc. In this paper, we focus on the design of the DMAs.



Citation: Wang, X.; Li, M.; Zhao, Y.; Wang, J.; Tan, X. Design of Planar Differential Microphone Array Beampatterns with Controllable Mainlobe Beamwidth and Sidelobe Level. *Sensors* 2023, 23, 3733. https://doi.org/10.3390/s23073733

Academic Editor: Iren E. Kuznetsova

Received: 17 February 2023 Revised: 25 March 2023 Accepted: 30 March 2023 Published: 4 April 2023



Copyright: © 2023 by the authors. Licensee MDPI, Basel, Switzerland. This article is an open access article distributed under the terms and conditions of the Creative Commons Attribution (CC BY) license (https://creativecommons.org/licenses/by/4.0/).

Sensors **2023**, 23, 3733 2 of 24

The concept of the DMA evolutes from the directional ribbon microphone [30,31] responding to the sound pressure gradient field instead of the sound pressure field. The gradient direction of the sound field is parallel with the propagating direction of the sound, and the maximum directional derivative is in the gradient direction of the sound field. This is the underlying reason why we usually assume that the desired signal comes from the end-fire direction for a linear microphone array. Traditionally, the DMAs are designed in a cascaded subtraction way [32–34] by using several small inter-element spacing omnidirectional microphones. Through adjusting the time delay among different channels, many classical beampatterns can be obtained, including cardioid, dipole, supercardioid and hypercardioid. Based on the cascaded subtraction structure, much of the literature has been devoted to the design and study of the DMAs from different perspectives [34–39]. However, the shortcoming of the cascaded subtraction structure is inflexible in dealing with the white noise amplification problem, which is the inherent problem of differential beamformers and is very serious at low-frequency bands. It limits the deployment of the DMAs in practice.

In order to overcome the aforementioned drawback, a so-called null-constrained method was developed recently in [27,40] in the frequency domain, which enables one to design DMAs by only using the distortionless and null constraints. Then, a minimum norm solution is deduced in this framework by using more microphones to design a lower order DMA, and the problem of white noise amplification can be solved to a certain extent [27,40]. In [28], it is shown that the null-constrained method is the same as the cascaded subtraction way, and the minimum norm solution is also explained in a two-stage manner. Based on the null-constrained method, many interesting differential beamformers have been studied and developed [24–26,41–44].

Though much research about DMA has been done, further research attention is indispensable. For example, it is known that the main lobe beamwidth of the beampattern of the classical differential beamformer is usually large, especially the low-order ones. However, a narrower main lobe may be preferred in some applications for better source acquisition. In addition, in some particular scenarios, if we do not want to distort the background noise field very much, beampattern with the same level sidelobes is favored. So, how to obtain a beamformer with a narrower main lobe and how to exactly control the main lobe beamwidth and sidelobe level to obtain frequency-invariant beampatterns with expected characteristics are very important in DMA context, and to the best of our knowledge, these are still open issues.

In this work, for overcoming the above problems, we resort to the Chebyshev polynomials in the design of planar differential microphone array, which has been widely used in traditional array design area [45–53]. The main contributions of this manuscript are as follows. First, via investigating the frequency-independent beampattern of a theoretical Nth-order differential beamformer, the desired beampattern is designed by exploiting the Chebyshev polynomials, whose main lobe beamwidth and sidelobe level can be exactly controlled, and the minimum main lobe beamwidth is guaranteed with a provided sidelobe level. Moreover, the relationship among the main lobe beamwidth, sidelobe level and polynomial order is deduced. Second, it has been proved theoretically in our framework that the first-order dipole beampattern has the narrowest beamwidth among the classical first-order differential beampatterns, i.e., dipole, cardioid, supercardioid and hypercardioid. Third, with the desired beampatterns at hands as targets, the so-called null constrained and least square beamformers for planar microphone array are proposed, which can obtain approximately frequency-invariant beampattern at relatively low frequencies and can be steered to any direction without beampattern distortion. Fourth, for overcoming the drawbacks of the null constrained and least square beamformers, i.e., severe white noise amplification problem at low frequencies and beampattern divergence from the desired one at high frequencies, the so-called minimum norm and combined solutions are deduced by exploiting the redundancy provided by using more microphones, which can flexibly compromise among the white noise gain (WNG), DF and beampattern divergence by

Sensors 2023, 23, 3733 3 of 24

adjusting parameters. Simulations are conducted and the preliminary results illustrate the properties and advantages of the proposed beamformers.

The remainder of this manuscript is as follows. The signal model, problem formulation and performance measures of beamforming are presented in Section 2. Section 3 introduces the approaches to the design of desired beampatterns. A set of differential beamformers are derived to approximate the desired beampatterns in Section 4. Simulations are conducted in Section 5, and conclusions are drawn in Section 6.

2. Signal Model, Problem Formulation and Performance Measures

The farfield plane wave model is considered in this manuscript. The microphone array consists of M omnidirectional microphones which are placed in a horizontal plane as shown in Figure 1. $(r_m \cos \theta_m, r_m \sin \theta_m)$ denotes the location of the mth sensor, whose radius and angle are denoted by r_m and θ_m , respectively. The desired source impinges on the microphone array from θ_s at the speed of sound $c \approx 343$ m/s. Obviously, the steering vector of the planar array is

$$\mathbf{d}(\omega, \theta_{s}) = \begin{bmatrix} e^{j\omega r_{1}\cos(\theta_{s} - \theta_{1})/c} & e^{j\omega r_{2}\cos(\theta_{s} - \theta_{2})/c} & \cdots & e^{j\omega r_{M}\cos(\theta_{s} - \theta_{M})/c} \end{bmatrix}^{T}, \tag{1}$$

where the superscript T is the transpose operator, $j = \sqrt{-1}$ is the imaginary unit, $\omega = 2\pi f$ is the angular frequency, f > 0 is the temporal frequency. Since the source is assumed to propagate from the angle θ_s , the signals observed by the microphone array are given by

$$\mathbf{y}(\omega) = [Y_1(\omega) Y_2(\omega) \cdots Y_M(\omega)]^T$$

$$= \mathbf{x}(\omega) + \mathbf{v}(\omega)$$

$$= \mathbf{d}(\omega, \theta_s) X(\omega) + \mathbf{v}(\omega), \tag{2}$$

where $Y_m(\omega)$ is the observed signal on mth microphone, $\mathbf{x}(\omega) = \mathbf{d}(\omega, \theta_s)X(\omega)$, $X(\omega)$ is the zero-mean desired signal, and $\mathbf{v}(\omega)$ is the zero-mean additive noise signal vector, which is defined similarly to $\mathbf{y}(\omega)$. The desired signal and additive noise are assumed to be uncorrelated with each other. The beamformer output is then [1]

$$Z(\omega) = \mathbf{h}^{H}(\omega)\mathbf{y}(\omega)$$

= $\mathbf{h}^{H}(\omega)\mathbf{d}(\omega, \theta_{s})X(\omega) + \mathbf{h}^{H}(\omega)\mathbf{v}(\omega),$ (3)

where $Z(\omega)$ is the estimate of the desired signal, $X(\omega)$,

$$\mathbf{h}(\omega) = [H_1(\omega) H_2(\omega) \cdots H_M(\omega)]^T$$
(4)

is a complex-valued linear filter applied to the observed signal vector, $\mathbf{y}(\omega)$, and the superscript H denotes conjugate-transpose. In our context, we do not want the desired signal to be distorted by the beamformer, so the distortionless constraint is desired, i.e.,

$$\mathbf{h}^{H}(\omega)\mathbf{d}(\omega,\theta_{s}) = 1. \tag{5}$$

The main interest of this work is beamforming with small inter-element spacing planar microphone arrays where the spacing between the neighboring microphones is much smaller than the minimum wavelength of the frequency band of interest. Consequently, the differentials of a different order of the acoustic pressure field can be approximated by finite differences in the microphones' output. Usually, the objective of differential beamforming is to design beamformers, i.e., to find beamforming filters, $\mathbf{h}(\omega)$, which response to the spatial derivative of acoustic pressure field of different orders, to estimate $X(\omega)$ as good as possible.

Sensors **2023**, 23, 3733 4 of 24

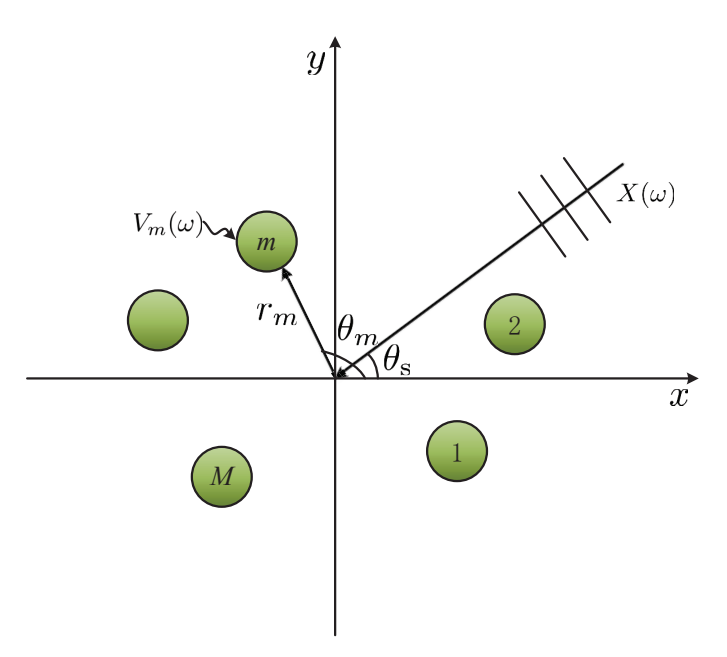


Figure 1. Illustration of a planar microphone array, where M is the microphone number, θ_s denotes the incidence angle of the desired source from farfield, r_m denotes the distance between the mth microphone and the coordinate system origin, and θ_m is the angle of the mth microphone.

Usually, the three most important performance measures, i.e., beampattern, WNG and DF, are used to evaluate the fixed beamformer.

The beampattern or directivity pattern describes the sensitivity of the beamformer to a plane wave impinging on the array from the direction θ . Mathematically, it is given by

$$\mathcal{B}[\mathbf{h}(\omega), \theta] = \mathbf{d}^{H}(\omega, \theta)\mathbf{h}(\omega)$$

$$= \sum_{m=1}^{M} H_{m}(\omega)e^{-j\omega r_{m}\cos(\theta - \theta_{m})/c}.$$
(6)

The null-to-null beamwidth of the beampattern is defined as the width between the two nulls which are closest to the main lobe from each side and is denoted by B_{NN} .

With the first microphone being the reference (without loss of generality), the input signal-to-noise ratio (iSNR) is defined as

$$iSNR(\omega) = \frac{\phi_X(\omega)}{\phi_{V_1}(\omega)},\tag{7}$$

where $\phi_X(\omega) = E[|X(\omega)|^2]$ and $\phi_{V_1}(\omega) = E[|V_1(\omega)|^2]$ are the variances of $X(\omega)$ and $V_1(\omega)$, respectively, and $E[\cdot]$ denotes the mathematical expectation. The output signal-tonoise ratio (oSNR), according to the beamforming model given in (3), is defined as

oSNR[
$$\mathbf{h}(\omega)$$
] = $\phi_X(\omega) \frac{\left|\mathbf{h}^H(\omega)\mathbf{d}(\omega, \theta_s)\right|^2}{\mathbf{h}^H(\omega)\mathbf{\Phi}_{\mathbf{v}}(\omega)\mathbf{h}(\omega)}$
= $\frac{\phi_X(\omega)}{\phi_{V_1}(\omega)} \times \frac{\left|\mathbf{h}^H(\omega)\mathbf{d}(\omega, \theta_s)\right|^2}{\mathbf{h}^H(\omega)\Gamma_{\mathbf{v}}(\omega)\mathbf{h}(\omega)}$, (8)

Sensors **2023**, 23, 3733 5 of 24

where $\Phi_{\mathbf{v}}(\omega) = E[\mathbf{v}(\omega)\mathbf{v}^H(\omega)]$ and $\Gamma_{\mathbf{v}}(\omega) = \frac{\Phi_{\mathbf{v}}(\omega)}{\phi_{V_1}(\omega)}$ are the correlation and pseudo-coherence matrices of $\mathbf{v}(\omega)$, respectively. The SNR gain derived from (7) and (8) is

$$G[\mathbf{h}(\omega)] = \frac{\text{oSNR}[\mathbf{h}(\omega)]}{\text{iSNR}(\omega)}$$

$$= \frac{\left|\mathbf{h}^{H}(\omega)\mathbf{d}(\omega, \theta_{s})\right|^{2}}{\mathbf{h}^{H}(\omega)\mathbf{\Gamma}_{\mathbf{v}}(\omega)\mathbf{h}(\omega)}.$$
(9)

Two particular types of noise are often considered for beamformer evaluation:

• Spatially and temporally white Gaussian noise with identical variances at all sensors, which models microphones' self-noise, nonuniform responses among the microphones, imperfections of the microphone positions, etc. In this scenario, $\Gamma_{\mathbf{v}}(\omega) = \mathbf{I}_M$, where \mathbf{I}_M is the identity matrix of size $M \times M$, and the resulting SNR gain is named as WNG, i.e.,

$$W[\mathbf{h}(\omega)] = \frac{\left|\mathbf{h}^{H}(\omega)\mathbf{d}(\omega, \theta_{s})\right|^{2}}{\mathbf{h}^{H}(\omega)\mathbf{h}(\omega)}.$$
(10)

So, the WNG evaluates the robust of the beamformer to some of the array imperfections. The maximum WNG that can be achieved by a beamforming filter is equal to M [40], i.e., $\mathcal{W}_{max} = M$. It can be obtained by the DS beamformer [40,54]:

$$\mathbf{h}_{\mathrm{DS}}(\omega) = \frac{\mathbf{d}(\omega, \theta_{\mathrm{s}})}{M}.\tag{11}$$

Note that $W[\mathbf{h}(\omega)] < 1$ indicates that there is white noise amplification.

Spherical isotropic noise, which is characterized by

$$[\mathbf{\Gamma}_{\mathrm{d}}(\omega)]_{ij} = \frac{\sin(\omega \delta_{ij}/c)}{\omega \delta_{ij}/c} = \mathrm{sinc}(\omega \delta_{ij}/c), \tag{12}$$

with $[\Gamma_{\rm d}(\omega)]_{mm}=1,\ m=1,\ 2,\ \ldots,\ M$, where δ_{ij} is the spacing between the ith and jth microphones. In this case, the SNR gain is named DF:

$$\mathcal{D}[\mathbf{h}(\omega)] = \frac{\left|\mathbf{h}^{H}(\omega)\mathbf{d}(\omega, \theta_{s})\right|^{2}}{\mathbf{h}^{H}(\omega)\mathbf{\Gamma}_{d}(\omega)\mathbf{h}(\omega)},\tag{13}$$

which quantifies how the beamformer performs in suppressing spatial directional noise, such as reverberation. The maximum DF that can be achieved by a beamformer with a given array is [40]

$$\mathcal{D}_{\text{max}}(\omega) = \mathbf{d}^{H}(\omega, \theta_{s}) \mathbf{\Gamma}_{d}^{-1}(\omega) \mathbf{d}(\omega, \theta_{s}), \tag{14}$$

which can be obtained by the so-called superdirective (hypercardioid) beamformer:

$$\mathbf{h}_{S}(\omega) = \frac{\Gamma_{d}^{-1}(\omega)\mathbf{d}(\omega, \theta_{s})}{\mathbf{d}^{H}(\omega, \theta_{s})\Gamma_{d}^{-1}(\omega)\mathbf{d}(\omega, \theta_{s})}.$$
(15)

It can be shown that [55], when the uniform linear array is considered, we have

$$\lim_{\delta \to 0} \mathcal{D}_{\max}(\omega) = M^2, \ \forall \omega, \tag{16}$$

which is referred as the supergain in the literature [56], and δ stands for the spacing between neighboring sensors.

Sensors **2023**, 23, 3733 6 of 24

3. Beampattern Design

It is well known that the frequency-independent beampattern of a theoretical Nth-order DMA whose main lobe is at $\theta = 0$ can be written as [32,40]

$$\mathcal{B}_N(\theta) = \sum_{n=0}^N a_{N,n} \cos^n \theta, \tag{17}$$

where $a_{N,n}$, n = 0, 1, ..., N, are real coefficients that determine the beampattern shape. For normalization, we would like the beampattern to be 1 in the direction of the main lobe, i.e., $\mathcal{B}_N(0) = 1$. So, we have

$$\sum_{n=0}^{N} a_{N,n} = 1. {(18)}$$

Different coefficients corresponding to different desired beampatterns of any order, such as classical dipole, cardioid, hypercardioid and supercardioid, can be found by optimizing different criteria [40,57], and one of the most important tasks of DMA design is to find desired beampattern and then approximate it as close as possible by beamforming filters.

While the aforementioned classical DMA beamformers have some optimum properties, there are some other issues. For example, the beamwidth of their beampattern is large usually, even for the hypercardioid beamformer which can obtain the maximum DF with a given microphone array. However, a narrower main lobe may be preferred in some applications for better source acquisition. In addition, in some particular scenarios, if we do not want to distort the background noise field very much, beampattern with the same level sidelobes is favored. So, in this manuscript, we try to exactly control the main lobe beamwidth and sidelobe level of the DMA beampattern.

From (17), we see that the beampattern, $\mathcal{B}_N(\theta)$, is a polynomial of order N which is symmetric about $\theta = 0$. In order to exactly control the main lobe beamwidth and sidelobe level and obtain minimum main lobe beamwidth with a given sidelobe level, we resort to the Chebyshev polynomials, which have been widely used in traditional array signal processing area [46,54].

The Chebyshev polynomials, $\mathcal{T}_N(x) = \cos\left(N\cos^{-1}x\right)$, are formed by using the Gram–Schmidt orthogonalization to the standard basis 1, x, x^2 , x^3 , ... in the interval $x \in [-1, 1]$ with respect to the weighting function $w(x) = 1/\sqrt{1-x^2}$ [41], where $\cos^{-1}x$ is the inverse function of $\cos x$. The first eight Chebyshev polynomials are [54]:

$$\mathcal{T}_0(x) = 1,$$

$$\mathcal{T}_1(x) = x,$$

$$\mathcal{T}_2(x) = 2x^2 - 1,$$

$$\mathcal{T}_3(x) = 4x^3 - 3x,$$

$$\mathcal{T}_4(x) = 8x^4 - 8x^2 + 1,$$

$$\mathcal{T}_5(x) = 16x^5 - 20x^3 + 5x,$$

$$\mathcal{T}_6(x) = 32x^6 - 48x^4 + 18x^2 - 1,$$

$$\mathcal{T}_7(x) = 64x^7 - 112x^5 + 56x^3 - 7x.$$

and for $N \ge 2$, we have

$$T_N(x) = 2xT_{N-1}(x) - T_{N-2}(x).$$
 (19)

Sensors **2023**, 23, 3733 7 of 24

The Chebyshev polynomials are a set of functions that are orthogonal in [-1, 1] with respect to the weighting function w(x) [41], i.e.,

$$\int_{-1}^{1} \frac{1}{\sqrt{1-x^2}} \mathcal{T}_n(x) \mathcal{T}_m(x) dx = c_n \delta(n-m), \tag{20}$$

where $\delta(\cdot)$ is the Dirac delta function, and c_n is

$$c_n = \begin{cases} \pi, & n = 0 \\ \pi/2, & n \neq 0 \end{cases}$$
 (21)

The definition of the *N*th degree Chebyshev polynomial on the whole range of *x* is

$$\mathcal{T}_N(x) = \begin{cases}
\cos\left(N\cos^{-1}x\right), & |x| \le 1 \\
\cosh\left(N\cosh^{-1}x\right), & x > 1 \\
(-1)^N\cosh\left(N\cosh^{-1}x\right), & x < -1
\end{cases} \tag{22}$$

where $\cosh^{-1} x$ is the inverse function of $\cosh x$.

 $\mathcal{T}_N(x)$ has N real roots in $x \in [-1, 1]$. By taking $x = \cos \theta$, we know that the roots are at $\cos(N\theta) = 0$, i.e.,

$$N\theta = (2k-1)\frac{\pi}{2}, \ 1 \le k \le N.$$
 (23)

From (22), we know that the Chebyshev polynomials have equal ripple characteristics in the interval [-1, 1] (the magnitude of every maxima and minima is 1, i.e., $|\mathcal{T}_N(x)| \le 1$), and all of the polynomials pass through the points (1, 1) and $(-1, (-1)^N)$. When |x| > 1, we have $|\mathcal{T}_N(x)| > 1$.

We assume the magnitude of the main lobe corresponds to the value of $\mathcal{T}_N(x_0)$ where $x_0 > 1$. The ratio of the main lobe level to the sidelobe level is defined as R, i.e.,

$$R = \frac{L_m}{L_c},\tag{24}$$

where L_m and L_s denote the main lobe level and sidelobe level, respectively. So, the point (x_0, R) on the $\mathcal{T}_N(x)$ curve is the position of the mainlobe maximum. According to (22), we have

$$x_0 = \cosh\left(\frac{1}{N}\cosh^{-1}R\right). \tag{25}$$

If we simply use $x = \cos \theta$, then $|x| \le 1$. However, in order to design the desired beampattern, we should utilize the entire range $[-1, x_0]$ of the Chebyshev polynomial [46,54]. So, we assume

$$x = c_1 \cos \theta + c_2, \tag{26}$$

where c_1 and c_2 are constant values. The range $[-1, x_0]$ in x-space corresponds to the range $[0, \pi]$ in θ -space. So, in order to control the whole range of the beampattern, i.e., $\theta \in [0, \pi]$, the mapping relationship presented in Table 1 should be satisfied [46].

Table 1. The Mapping Relationship Between θ and x.

θ	0	π
$x = c_1 \cos \theta + c_2$	x_0	-1

Sensors **2023**, 23, 3733 8 of 24

To determine c_1 and c_2 , we solve the following two equations:

$$c_1 + c_2 = x_0,$$

$$-c_1 + c_2 = -1,$$

and have

$$c_1 = \frac{x_0 + 1}{2}, c_2 = \frac{x_0 - 1}{2}.$$
 (27)

Substituting (27) into (26), we have

$$x = \frac{x_0 + 1}{2}\cos\theta + \frac{x_0 - 1}{2}. (28)$$

So, the desired beampattern is

$$\mathcal{B}_{N,d}(\theta) = \frac{1}{R} \mathcal{T}_N\left(\frac{x_0 + 1}{2}\cos\theta + \frac{x_0 - 1}{2}\right),\tag{29}$$

where the factor 1/R normalizes the beampattern making $\mathcal{B}_N(0) = 1$. Obviously, we can steer the desired beampattern to θ_s as

$$\mathcal{B}_{N,d}(\theta - \theta_{s}) = \frac{1}{R} \mathcal{T}_{N} \left[\frac{x_{0} + 1}{2} \cos\left(\theta - \theta_{s}\right) + \frac{x_{0} - 1}{2} \right]. \tag{30}$$

For conciseness, in this section, we only discuss the case of $\theta_s = 0$, i.e., the desired beampattern in (29). A simple beampattern steering method will be given in the next section. From (23), we know that the roots of $\mathcal{T}_N(\cos\theta)$ are

$$\theta_k = \frac{(2k-1)\pi}{2N}, \ 1 \le k \le N.$$
 (31)

So, in *x*-space the roots are at

$$x = \frac{x_0 + 1}{2}\cos\theta + \frac{x_0 - 1}{2} = \cos\theta_k. \tag{32}$$

Then, we know the roots in the scaled space occur at

$$\theta_{k0} = \cos^{-1}\left[\frac{2}{x_0 + 1}\left(\cos\theta_k - \frac{x_0 - 1}{2}\right)\right], k = 1, 2, \dots, N.$$
 (33)

From (33), we know the main lobe beamwidth is

$$B_{\text{NN}} = 2\theta_{10} = 2\cos^{-1}\left[\frac{2}{x_0 + 1}\left(\cos\frac{\pi}{2N} - \frac{x_0 - 1}{2}\right)\right]. \tag{34}$$

By simple manipulation, we obtain

$$B_{\text{NN}} = 2\cos^{-1}\left[\frac{2}{x_0 + 1}\left(\cos\frac{\pi}{2N} + 1\right) - 1\right]$$

$$= 2\cos^{-1}\left[\frac{2}{\cosh\left(\frac{1}{N}\cosh^{-1}R\right) + 1}\left(\cos\frac{\pi}{2N} + 1\right) - 1\right]. \tag{35}$$

Since $x_0 > 1$ and $N \ge 1$, we have

$$-1 < \frac{2}{x_0 + 1} \left(\cos \frac{\pi}{2N} + 1 \right) - 1 < 1. \tag{36}$$

Sensors 2023, 23, 3733 9 of 24

So, we can observe that the beamwidth, $B_{\rm NN}$, increases with R (which increases with the increase of x_0) and decreases with N. Consequently, we can make a compromise between the main lobe beamwidth and sidelobe level with a provided N flexibly. When N is given, the main lobe beamwidth can be adjusted by tuning R, and the minimum beamwidth is obtained when $R \to 1$ (i.e., $x_0 \to 1$), which means the magnitudes of the main lobe and sidelobe are the same, and we have

$$\lim_{R \to 1} B_{\text{NN}} = \frac{\pi}{N}.\tag{37}$$

So, the 1st order dipole beampattern, which has the same magnitudes of the main lobe and sidelobe and a null at $\pi/2$, has the minimum main lobe beamwidth, i.e., $B_{\rm NN}=\pi$, among the different 1st order DMA beampatterns.

From (35), we can also get

$$R = \cosh \left\{ N \cosh^{-1} \left[\frac{2(\cos \frac{\pi}{2N} + 1)}{\cos \frac{B_{NN}}{2} + 1} - 1 \right] \right\}, \tag{38}$$

i.e., when N and $B_{\rm NN}$ are given, we can determine R using (38). However, it should be noted that the $B_{\rm NN}$ will never be narrower than π/N . The method of designing the desired beampattern is described in Algorithm 1.

Algorithm 1: Steps for designing the desired beampattern.

- 1: Select the order, N, of the desired beampattern, $\mathcal{B}_N(\theta)$, and choose the Chebyshev polynomial, $\mathcal{T}_N(x)$, of the same order;
- 2: Set the ratio of the main lobe level to the sidelobe level, R, and determine x_0 according to (25), or set the main lobe beamwidth B_{NN} , and determine the parameter R according to (38) and then find x_0 ;
- 3: Change the scale by using the mapping function (28);
- 4: Obtain the desired beampattern, $\mathcal{B}_{N,d}(\theta)$, according to (29) (the methods of approximating the desired beampattern are described in Section 4).

It is observed that, from (35), we can calculate the order of the Chebyshev polynomial, $N_{\rm F}$, by using numerical methods when $B_{\rm NN}$ and R are given, where the subscript 'F' denotes fractional. Though the polynomial order N should be an integer, $N_{\rm F}$ gives us a good reference.

As seen, (29) can be rewritten as

$$\mathcal{B}_{N,d}(\theta) = \frac{1}{R} \mathcal{T}_N \left[\frac{x_0 + 1}{4} (e^{j\theta} + e^{-j\theta}) + \frac{x_0 - 1}{2} \right], \tag{39}$$

and the component $e^{-j\omega r_m\cos(\theta-\theta_m)/c}$ in (6) can be expressed as a function of $e^{-jn\theta}$ using the Jacobi-Anger expansion [58,59]. Consequently, we can deduce the beamformer coefficients by solving the following equation:

$$\mathcal{B}[\mathbf{h}(\omega), \theta] = \mathcal{B}_{N,\mathbf{d}}(\theta). \tag{40}$$

However, it is difficult when N is large. So, for simplicity, we proposed the so-called null-constrained and least square beamformers in the next section.

4. DMA Design

With the desired beampattern, $\mathcal{B}_{N,d}(\theta)$, at hand as target, our task is to approximate it as close as possible. In this work, we first introduce two kinds of methods, i.e., null-constrained and least square methods. Then, we derive the minimum norm and combined solutions in order to improve the white noise amplification problem at low-frequency

bands and prevent the array beampattern from significantly deviating from the desired one at high-frequency bands.

From (17), we know the desired beampattern is symmetric about the $0 \leftrightarrow \pi$ axis. However, to design the beampattern of the planar array, we need to consider the whole range of θ , i.e., $\theta \in [0, 2\pi]$. So, 2N zeros are taken in to account in our context, i.e., θ_{k0} , $k=1, 2, \ldots, 2N$. The first N zeros are θ_{k0} , $k=1, 2, \ldots, N$, and the last N zeros are $2\pi - \theta_{k0}$, $k=1, 2, \ldots, N$. It should be noted that, since $\mathcal{T}_N(x)$ pass through the point $(-1, (-1)^N)$, we will never have a null at $\theta = \pi$, with a given limited R. So, there is not higher (than 1) order null.

4.1. Null Constrained Method

As known, the position of nulls is very important in DMA design, which determines the beampattern of DMA uniquely [27,40]. In this part, we assume $M = M_N = 2N + 1$, where M_N is the minimum microphone number that is required to form a Nth order planar DMA beampattern given the array geometry. By combining the distortionless constraint (which is at $\theta = 0$) and the null constraints, we have the following linear system:

$$\mathbf{D}(\omega, \boldsymbol{\theta}_0)\mathbf{h}(\omega) = \mathbf{i}_{M_{\mathrm{M}}},\tag{41}$$

where

$$\mathbf{D}(\omega, \boldsymbol{\theta}_0) = \begin{bmatrix} \mathbf{d}^H(\omega, 0) \\ \mathbf{d}^H(\omega, \boldsymbol{\theta}_{10}) \\ \mathbf{d}^H(\omega, \boldsymbol{\theta}_{20}) \\ \vdots \\ \mathbf{d}^H(\omega, \boldsymbol{\theta}_{N0}) \\ \vdots \\ \mathbf{d}^H(\omega, \boldsymbol{\theta}_{2N0}) \end{bmatrix}$$
(42)

is the constraint matrix of size $M_N \times M_N$, which is assumed to be a full rank matrix, $\theta_0 = [\theta_{10}, \theta_{20}, \cdots, \theta_{N0}, \cdots, \theta_{2N0}]$ and \mathbf{i}_{M_N} is the first column of the identity matrix, \mathbf{I}_{M_N} , of size $M_N \times M_N$. So, we can obtain the beamformer as

$$\mathbf{h}_{\mathrm{NC}}(\omega) = \mathbf{D}^{-1}(\omega, \boldsymbol{\theta}_0) \mathbf{i}_{M_N}. \tag{43}$$

If we want to steer the main lobe to directions other than $\theta=0$, the nulls can be set at $\theta_0=[\theta_s+\theta_{10}, \theta_s+\theta_{20}, \cdots, \theta_s+\theta_{N0}, \cdots, \theta_s+\theta_{2N0}]$, and now the distortionless constraint is $\mathbf{d}^H(\omega,\theta_s)\mathbf{h}(\omega)=1$, where θ_s is the steered direction.

4.2. Least Square Method

In this part, again, we assume $M=M_N$. Let us define the error of the DMA beampattern first:

$$\mathcal{E}[\mathbf{h}(\omega), \, \theta] = \mathcal{B}_{N,\mathbf{d}}(\theta) - \mathcal{B}[\mathbf{h}(\omega), \theta]$$
$$= \mathcal{B}_{N,\mathbf{d}}(\theta) - \mathbf{d}^{H}(\omega, \theta)\mathbf{h}(\omega). \tag{44}$$

Then, the least square approximation criterion [41] can be written as

$$J_{LS}[\mathbf{h}(\omega)] = \int_{0}^{2\pi} |\mathcal{E}[\mathbf{h}(\omega), \, \theta]|^{2} d\theta$$

$$= \mathbf{h}^{H}(\omega)\mathbf{P}(\omega)\mathbf{h}(\omega) - \mathbf{h}^{H}(\omega)\mathbf{q}(\omega) - \mathbf{q}^{H}(\omega)\mathbf{h}(\omega) + \int_{0}^{2\pi} |\mathcal{B}_{N,d}(\theta)|^{2} d\theta, \quad (45)$$

where

$$\mathbf{P}(\omega) = \int_0^{2\pi} \mathbf{d}(\omega, \theta) \mathbf{d}^H(\omega, \theta) d\theta,$$
$$\mathbf{q}(\omega) = \int_0^{2\pi} \mathcal{B}_{N, \mathbf{d}}(\theta) \mathbf{d}(\omega, \theta) d\theta$$

are matrices of size $M_N \times M_N$ and $M_N \times 1$, respectively. Of course, we can use a weighting function to either emphasize or deemphasize some specific angles. However, for simplicity, we set the weighting function to 1 in this work. By combining $J_{LS}[\mathbf{h}(\omega)]$ and the distortionless constraint, we obtain the cost function, i.e.,

$$\min_{\mathbf{h}(\omega)} J_{\mathrm{LS}}[\mathbf{h}(\omega)] \text{ subject to } \mathbf{d}^{H}(\omega, 0)\mathbf{h}(\omega) = 1. \tag{46}$$

Solving (46) by using the Lagrange multiplier method, the beamformer is derived as

$$\mathbf{h}_{\mathrm{LS}}(\omega) = \frac{\mathbf{P}^{-1}(\omega)\mathbf{q}(\omega)}{\mathbf{q}^{H}(\omega)\mathbf{P}^{-1}(\omega)\mathbf{d}(\omega,0)}.$$
 (47)

In this case, if we want to steer the main lobe to direction $\theta_s \neq 0$, we can set the desired beampattern as in (30).

4.3. Minimum Norm Solution

In the traditional and the above DMA design routines, it is assumed that $M=M_N$. As known, one of the inherent shortcomings of the differential beamformer is the white noise amplification problem at low-frequency bands. Recently, in order to improve this thorny problem, the minimum norm solution is proposed in [40,57] which takes the advantage that we can exploit the redundancy by using more microphones, i.e., $M>M_N$. In this context, the linear system can be written as

$$\overline{\mathbf{D}}(\omega, \boldsymbol{\theta}_0)\mathbf{h}(\omega) = \mathbf{i}_{M_N},\tag{48}$$

where

$$\overline{\mathbf{D}}(\omega, \boldsymbol{\theta}_{0}) = \begin{bmatrix}
\overline{\mathbf{d}}^{H}(\omega, 0) \\
\overline{\mathbf{d}}^{H}(\omega, \boldsymbol{\theta}_{10}) \\
\overline{\mathbf{d}}^{H}(\omega, \boldsymbol{\theta}_{20}) \\
\vdots \\
\overline{\mathbf{d}}^{H}(\omega, \boldsymbol{\theta}_{N0}) \\
\vdots \\
\overline{\mathbf{d}}^{H}(\omega, \boldsymbol{\theta}_{2N0})
\end{bmatrix}$$
(49)

is the constraint matrix of size $M_N \times M$, which is assumed to be a row full rank matrix, and $\overline{\mathbf{d}}(\omega,\theta)$ is the steering vector of length $M>M_N$. Then, the minimum norm solution can be derived by solving the following cost function:

$$\min_{\mathbf{h}(\omega)} \mathbf{h}^{H}(\omega)\mathbf{h}(\omega) \text{ subject to } \overline{\mathbf{D}}(\omega, \boldsymbol{\theta}_{0})\mathbf{h}(\omega) = \mathbf{i}_{M_{N}}, \tag{50}$$

and the beamforming filter is

$$\mathbf{h}_{\mathrm{MN}}(\omega) = \overline{\mathbf{D}}^{H}(\omega, \boldsymbol{\theta}_{0}) \left[\overline{\mathbf{D}}(\omega, \boldsymbol{\theta}_{0}) \overline{\mathbf{D}}^{H}(\omega, \boldsymbol{\theta}_{0}) \right]^{-1} \mathbf{i}_{M_{N}}. \tag{51}$$

4.4. Combined Solution

Usually, at relatively high-frequency bands (compared to the spacing between the neighboring sensors), the array beampattern significantly deviates from the desired one since the differentials of a different order of the acoustic pressure field can no longer be approximated precisely by finite difference of the microphones' output when the microphone array geometry is given. So, it is necessary to control the distortion of the beampattern and the white noise amplification problem simultaneously. Consequently, we apply the following cost function [41]:

$$\min_{\mathbf{h}(\omega)} \mu \mathbf{h}^{H}(\omega) \mathbf{h}(\omega) + (1 - \mu) J_{LS}[\mathbf{h}(\omega)] \text{ subject to } \overline{\mathbf{D}}(\omega, \boldsymbol{\theta}_{0}) \mathbf{h}(\omega) = \mathbf{i}_{M_{N}},$$
 (52)

and the solution which is named a combined solution is

$$\mathbf{h}_{\mathsf{C}}(\omega) = \overline{\mathbf{P}}_{\mu}^{-1}(\omega) \Big\{ 2(1-\mu)\overline{\mathbf{q}}(\omega) + \overline{\mathbf{D}}^{H}(\omega, \boldsymbol{\theta}_{0})\overline{\mathbf{Q}}_{\mu}^{-1}(\omega) \Big[\mathbf{i}_{M_{N}} - 2(1-\mu)\overline{\mathbf{D}}(\omega, \boldsymbol{\theta}_{0})\overline{\mathbf{P}}_{\mu}^{-1}(\omega)\overline{\mathbf{q}}(\omega) \Big] \Big\}, \tag{53}$$

where

$$\begin{split} & \overline{\mathbf{P}}_{\mu}(\omega) = 2\mu \mathbf{I}_{M} + 2(1-\mu)\overline{\mathbf{P}}(\omega), \\ & \overline{\mathbf{Q}}_{\mu}(\omega) = \overline{\mathbf{D}}(\omega, \boldsymbol{\theta}_{0})\overline{\mathbf{P}}_{\mu}^{-1}(\omega)\overline{\mathbf{D}}^{H}(\omega, \boldsymbol{\theta}_{0}), \\ & \overline{\mathbf{P}}(\omega) = \int_{0}^{2\pi} \overline{\mathbf{d}}(\omega, \theta)\overline{\mathbf{d}}^{H}(\omega, \theta)d\theta, \\ & \overline{\mathbf{q}}(\omega) = \int_{0}^{2\pi} \mathcal{B}_{N,d}(\theta)\overline{\mathbf{d}}(\omega, \theta)d\theta \end{split}$$

are of size $M \times M$, $M_N \times M_N$, $M \times M$ and $M \times 1$, respectively, and $0 \le \mu \le 1$. When $\mu = 1$, we get the minimum norm solution, $\mathbf{h}_{MN}(\omega)$.

For more degree of freedom to deal with the white noise amplification problem at low frequencies, we simplify (52) as [41]

$$\min_{\mathbf{h}(\omega)} \mu \mathbf{h}^{H}(\omega) \mathbf{h}(\omega) + (1 - \mu) J_{LS}[\mathbf{h}(\omega)] \text{ subject to } \overline{\mathbf{d}}^{H}(\omega, 0) \mathbf{h}(\omega) = 1,$$
 (54)

whose solution is

$$\mathbf{h}_{\mathrm{CF}}(\omega) = \overline{\mathbf{P}}_{\mu}^{-1}(\omega) \left[2(1-\mu)\overline{\mathbf{q}}(\omega) + \frac{1-2(1-\mu)\overline{\mathbf{d}}^{H}(\omega)\overline{\mathbf{P}}_{\mu}^{-1}(\omega)\overline{\mathbf{q}}(\omega)}{\overline{\mathbf{d}}^{H}(\omega)\overline{\mathbf{P}}_{\mu}^{-1}(\omega)\overline{\mathbf{d}}(\omega)} \overline{\mathbf{d}}(\omega) \right]. \tag{55}$$

When $\mu=0$, we get the least square beamformer, $\mathbf{h}_{LS}(\omega)$, with redundant microphone, and when $\mu=1$, we get the delay-and-sum beamformer, $\mathbf{h}_{DS}(\omega)$.

4.5. Particular Case: Linear Microphone Array

The methods proposed above are applicable to linear microphone arrays. However, for a linear array, we only need to consider the range $\theta \in [0, \pi]$. In this case, the microphone number M is require to satisfy $M \geq M_{N,L} = N+1$, $\theta_0 = [\theta_{10}, \theta_{20}, \cdots, \theta_{N0}]$, and $\mathbf{D}(\omega, \theta_0)$ of size $M_{N,L} \times M_{N,L}$ and $\overline{\mathbf{D}}(\omega, \theta_0)$ of size $M_{N,L} \times M$ are, respectively,

$$\mathbf{D}(\omega, \boldsymbol{\theta}_0) = \begin{bmatrix} \mathbf{d}^H(\omega, 0) \\ \mathbf{d}^H(\omega, \boldsymbol{\theta}_{10}) \\ \mathbf{d}^H(\omega, \boldsymbol{\theta}_{20}) \\ \vdots \\ \mathbf{d}^H(\omega, \boldsymbol{\theta}_{N0}) \end{bmatrix}$$
(56)

and

$$\overline{\mathbf{D}}(\omega, \boldsymbol{\theta}_{0}) = \begin{bmatrix} \overline{\mathbf{d}}^{H}(\omega, 0) \\ \overline{\mathbf{d}}^{H}(\omega, \boldsymbol{\theta}_{10}) \\ \overline{\mathbf{d}}^{H}(\omega, \boldsymbol{\theta}_{20}) \\ \vdots \\ \overline{\mathbf{d}}^{H}(\omega, \boldsymbol{\theta}_{N0}) \end{bmatrix}. \tag{57}$$

It should be noted that the steering ability of the linear DMA is limited [60–62].

5. Simulations

In this section, we evaluate the performance of the methods proposed above.

5.1. Desired Beampattern

We first study the desired beampattern with a different main lobe level to sidelobe level ratio R. The order of the Chebyshev polynomial is set to be N=3, and R=5, 10, 20 and 30 (in dB, the same below) are considered. The results are presented in Figure 2. As seen, the sidelobe level is controlled precisely, and the main lobe beamwidth increases with the increase of R. When R is small, the main lobe beamwidth is narrower than that of the superdirective beamformer (whose beampattern can be found in [21,27]) Next, we investigate the beampatterns with a given main lobe beamwidth $B_{\rm NN}=\pi/3$ and different polynomial order N (N=4,5,6,7). The beampatterns are plotted in Figure 3. It is observed that we can exactly control the main lobe beamwidth if the polynomial order N is adequate.

Then, we evaluate the performance of the beamformers proposed in Section 4.

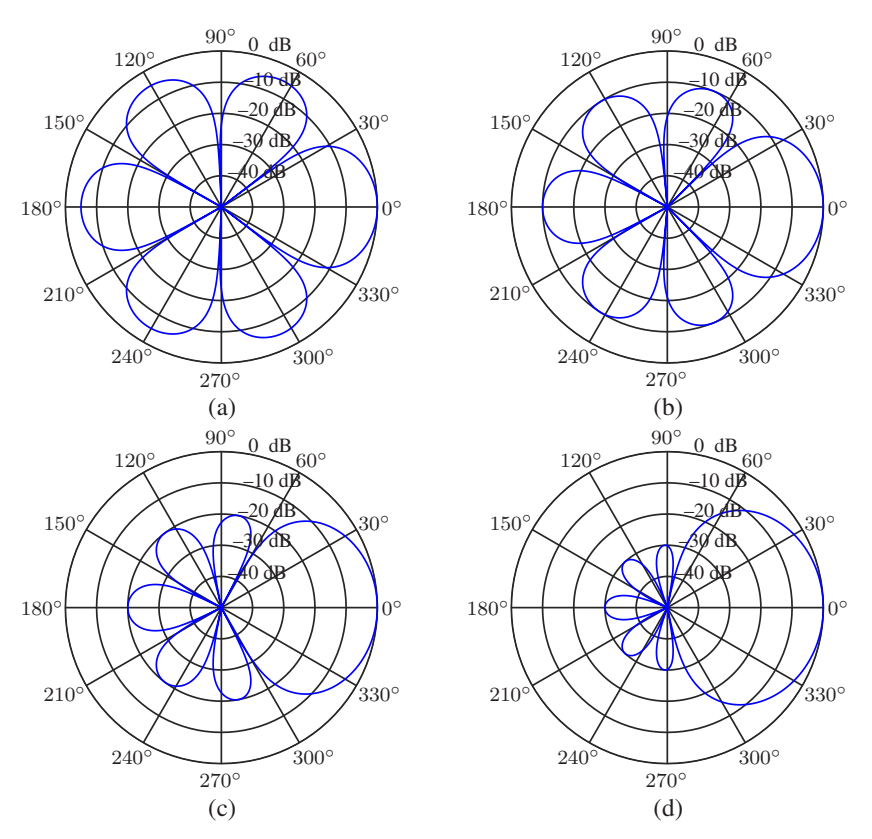


Figure 2. Desired beampatterns with different ratio, R, of mainlobe level to sidelobe level: (a) R = 5, (b) R = 10, (c) R = 20, and (d) R = 30. Conditions: N = 3, and $\theta_s = 0$.

Sensors **2023**, 23, 3733 14 of 24

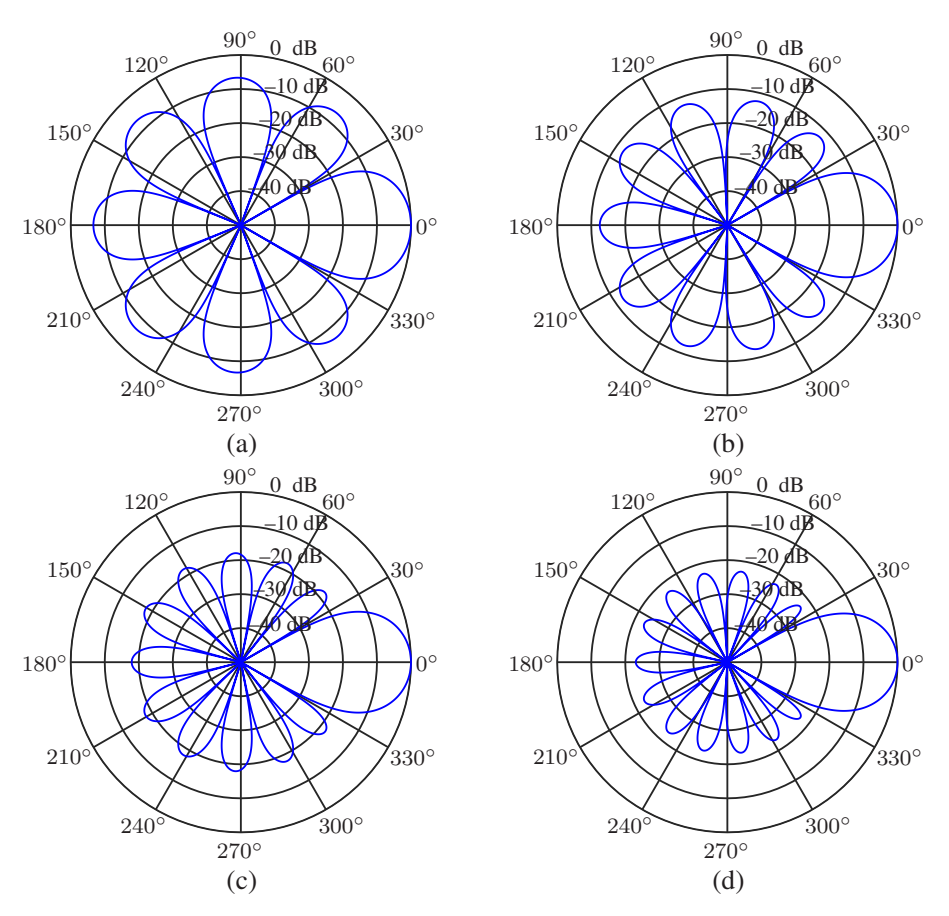


Figure 3. Desired beampatterns with a given mainlobe beamwidth B_{NN} and different polynomial order N: (a) N=4, (b) N=5, (c) N=6, and (d) N=7. Conditions: $B_{NN}=\pi/3$ and $\theta_s=0$.

5.2. Performance of the Null Constrained and Least Square Beamformers

The uniform circular array (UCA) is considered in the performance evaluation parts. The null-constrained beamformer is studied first. Again, the order of the Chebyshev polynomial is set to be N=3, and R=30 (dB) is taken, i.e., the desired beampattern that we want to approximate is Figure 2d. So, M = 7 microphones are needed. The radius of the UCA is set to be r = 0.02 m. The beampatterns of the null-constrained beamformer with different frequencies (f = 500, 1000, 2000 and 4000 Hz) are shown in Figure 4, including the beampattern of the maximum front-to-back ratio [63] (purple dot line) beamformer at $f=1000~\mathrm{Hz}$. We can see from Figure 4 that, at relatively low frequencies, the beampattern of the null-constrained beamformer is very close to the desired one. However, at high frequencies, the array beampattern diverges from the desired beampattern gradually, and the divergence increases with the increase of frequency. The reason has been explained in Section 4.4. In addition, as we can see from Figure 4b, comparing with the beampattern of the maximum front-to-back ratio beamformer, the sidelobe level of $\mathbf{h}_{NC}(\omega)$ is exactly controlled, and the level of different sidelobe is the same, which is useful if we do not want to distort the background noise field too much. Figure 5 plots the 3-D beampattern of the null constrained beamformer versus frequency with $\theta_s = 0$. We can see that the beampattern is approximate frequency-invariant at low frequencies, and the sidelobe level gradually increases with the increase of frequency at high frequencies.

Sensors **2023**, 23, 3733 15 of 24

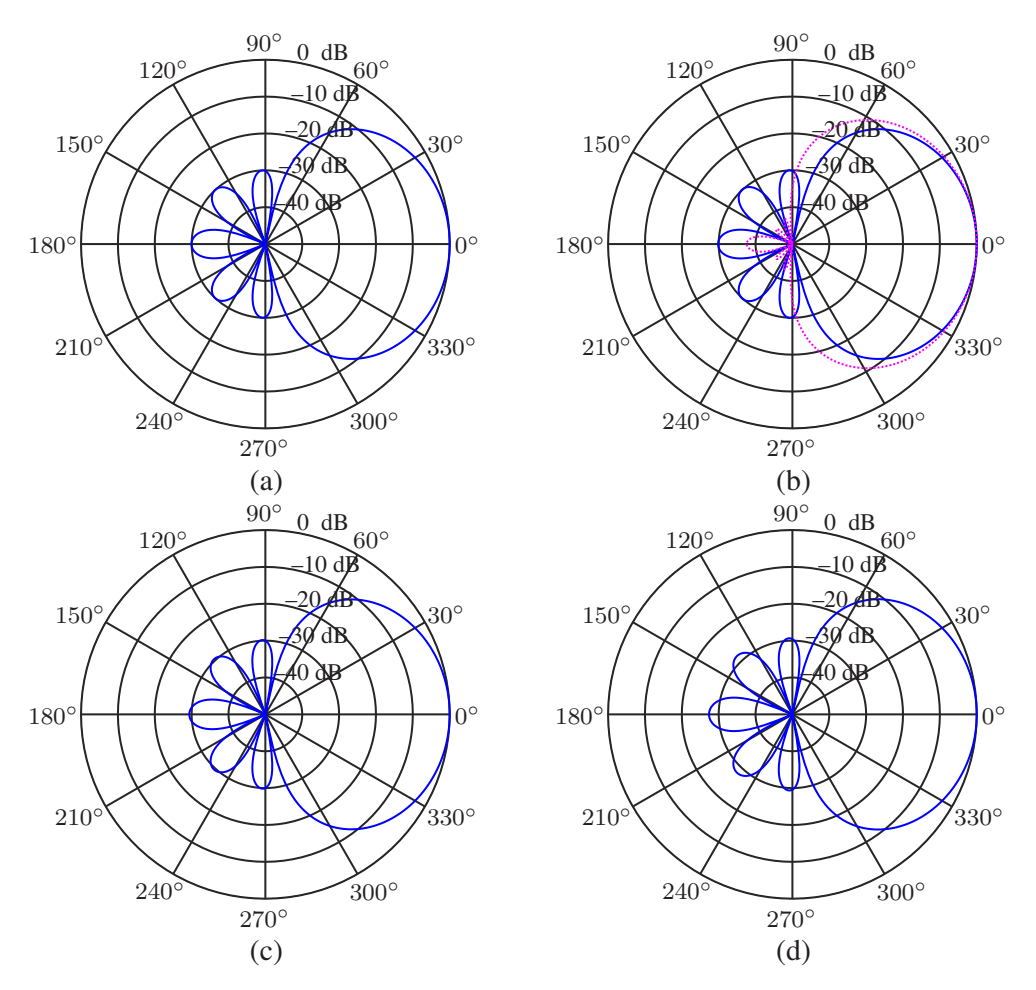


Figure 4. Beampatterns of the null constrained beamformer, $\mathbf{h}_{NC}(\omega)$, with different frequencies: (a) f = 500 Hz, (b) f = 1000 Hz, (c) f = 2000 Hz, and (d) f = 4000 Hz. Conditions: N = 3, M = 7, R = 30, r = 0.02 m, and $\theta_S = 0$.

For evaluating the performance of the beamformer $h_{NC}(\omega)$, we simulated the room acoustic environments with the well-known image model [64,65]. The sampling rate is set to 8 kHz. The length, width and height of the simulated room are, respectively, 4 m, 4 m and 3 m. The position of the point in the simulated room is denoted as (x, y, z) with respect to a corner of the room which is considered the origin of the Cartesian coordinate system. A UCA with radius r = 0.02 m and 7 microphones, whose center and the first microphone are at (2, 2, 1.5) (in meter, the same below) and (2.02, 2, 1.5), respectively, is considered in the simulation. The main lobe level to sidelobe level ratio, R, is set to 20 dB. 360 loudspeakers are simulated as sources of interest and placed at the same horizontal plane of the UCA with 1° interval, and the distance between the loudspeakers and the center of the UCA is 1.5 m. The reflection coefficients of all six walls are set to 0.40 and the corresponding reverberation time $T_{60} \approx 110$ ms. The room impulse responses (RIRs) between every microphone and loudspeaker are generated using the image model. The output signal of each microphone is generated by convoluting a piece of the clean speech signal with the simulated RIRs. The normalized energy of the output signal of the beamformer $h_{NC}(\omega)$ and $h_S(\omega)$ is presented in Figure 6. As seen from Figure 6, for input signal from different directions, the output energy of the beamformer $\mathbf{h}_{NC}(\omega)$ corresponding to the sidelobe region keeps flatter than that of the beamformer $\mathbf{h}_{S}(\omega)$.

Sensors 2023, 23, 3733 16 of 24

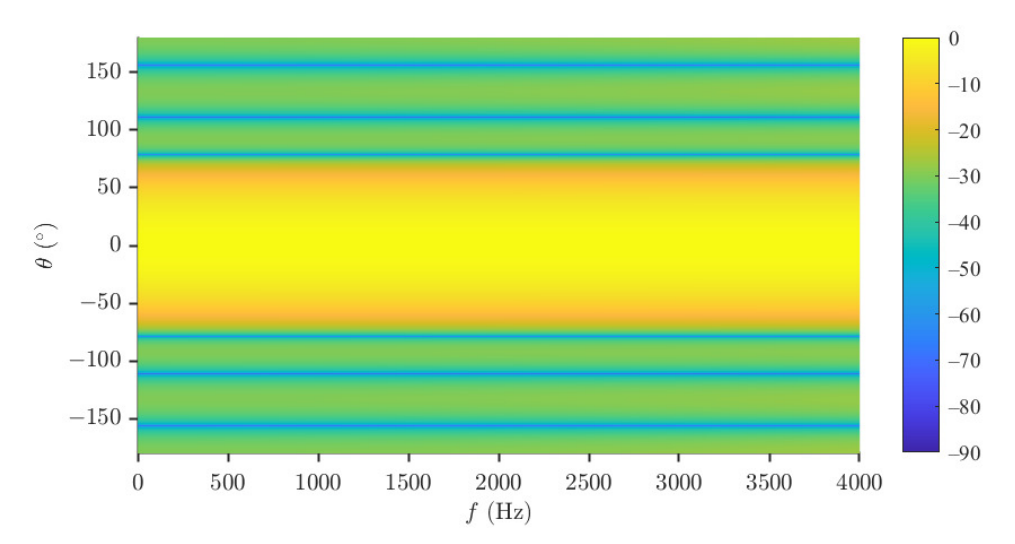


Figure 5. Beampattern of the null constrained beamformer, $\mathbf{h}_{NC}(\omega)$, versus frequency. Conditions: N=3, M=7, R=30, r=0.02 m, and $\theta_{S}=0$.

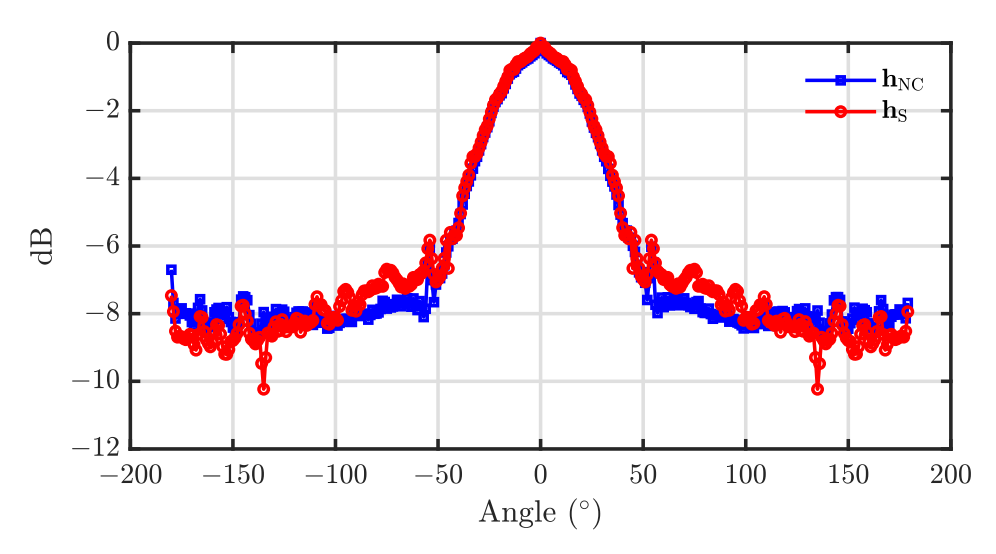


Figure 6. The normalized energy of the output signal of the beamformer $\mathbf{h}_{NC}(\omega)$ and $\mathbf{h}_{S}(\omega)$ for the input signal from different direction. Conditions: N = 3, M = 7, R = 20, r = 0.02 m, and $\theta_{S} = 0$.

Now, we take a look at the beampatterns of the least square beamformer. Again, we use the setting of N=3, R=30 (dB), M=7, and r=0.02 m. The resulting beampatterns are shown in Figure 7, from which we can see the same phenomenon, i.e., the array beampattern is similar to the desired one at low frequencies, and it diverges from the desired one at high frequencies.

Using the same array and Chebyshev polynomial parameters as the last simulation, we study the steering ability of the null-constrained and least square beamformers. Figure 8 describes the beampatterns of the beamformers $\mathbf{h}_{NC}(\omega)$ and $\mathbf{h}_{LS}(\omega)$ with different direction of the desired signal, $\theta_{\rm s}$ ($\theta_{\rm s}=30^\circ,60^\circ,90^\circ$ and 120°), at frequency f=1000 Hz. As we can see, the beampattern of the proposed two beamformers can be steered to any direction without distortion.

Sensors 2023, 23, 3733 17 of 24

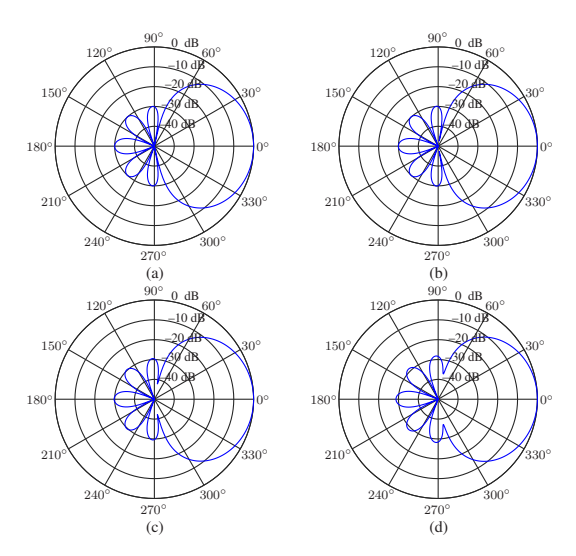


Figure 7. Beampatterns of the least square beamformer, $\mathbf{h}_{LS}(\omega)$, with different frequencies: (a) f = 500 Hz, (b) f = 1000 Hz, (c) f = 2000 Hz, and (d) f = 4000 Hz. Conditions: N = 3, M = 7, R = 30, r = 0.02 m, and $\theta_s = 0$.

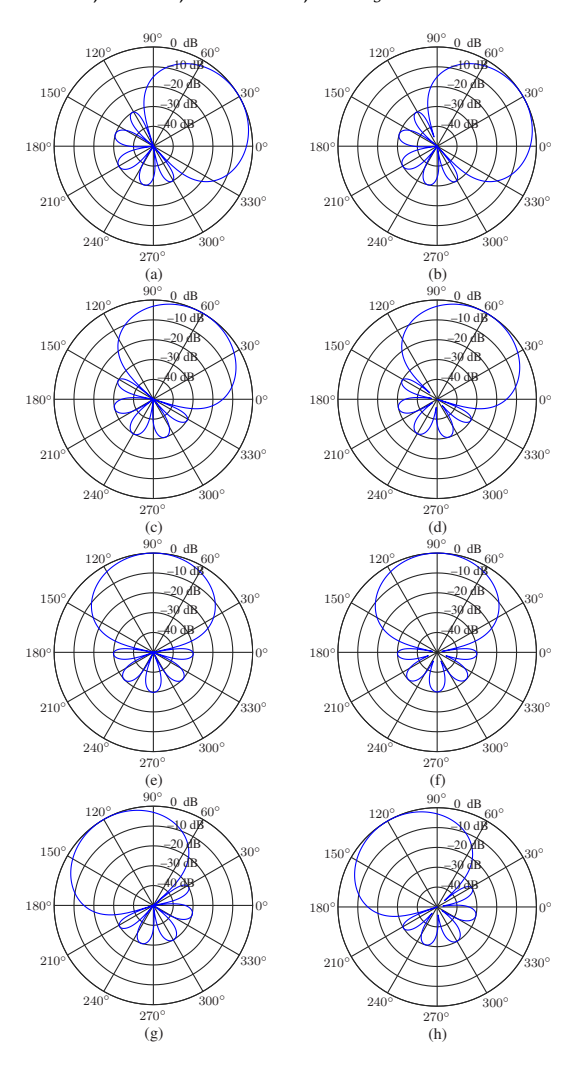


Figure 8. Beampatterns of the beamformers $\mathbf{h}_{NC}(\omega)$ and $\mathbf{h}_{LS}(\omega)$ with different values of θ_s : (a) $\mathbf{h}_{NC}(\omega)$, $\theta_s=30^\circ$, (b) $\mathbf{h}_{LS}(\omega)$, $\theta_s=30^\circ$, (c) $\mathbf{h}_{NC}(\omega)$, $\theta_s=60^\circ$, (d) $\mathbf{h}_{LS}(\omega)$, $\theta_s=60^\circ$, (e) $\mathbf{h}_{NC}(\omega)$, $\theta_s=90^\circ$, (f) $\mathbf{h}_{LS}(\omega)$, $\theta_s=90^\circ$, (g) $\mathbf{h}_{NC}(\omega)$, $\theta_s=120^\circ$, and (h) $\mathbf{h}_{LS}(\omega)$, $\theta_s=120^\circ$. Conditions: N=3, M=7, R=30, r=0.02 m, and f=1000 Hz.

Sensors 2023, 23, 3733 18 of 24

The WNG and DF of the null constrained and least square beamformers are investigated in our simulations, and the parameter settings are the same as in the last simulation. Figure 9 shows the WNG and DF with respect to R at f=1000 Hz, and the results of the DS and superdirective beamformers are also included. As seen, the DF of the null constrained and least square beamformers increase with R first and then decreases, which is always less than that of the superdirective beamformer as expected. The WNG, however, increases with R monotonically. The WNG and DF of $\mathbf{h}_{\rm NC}(\omega)$ and $\mathbf{h}_{\rm LS}(\omega)$ as functions of frequency with N=3 and R=30 are plotted in Figure 10. It is observed that the WNG is very low at low-frequency bands, which is the motivation of the development of the minimum norm solution.

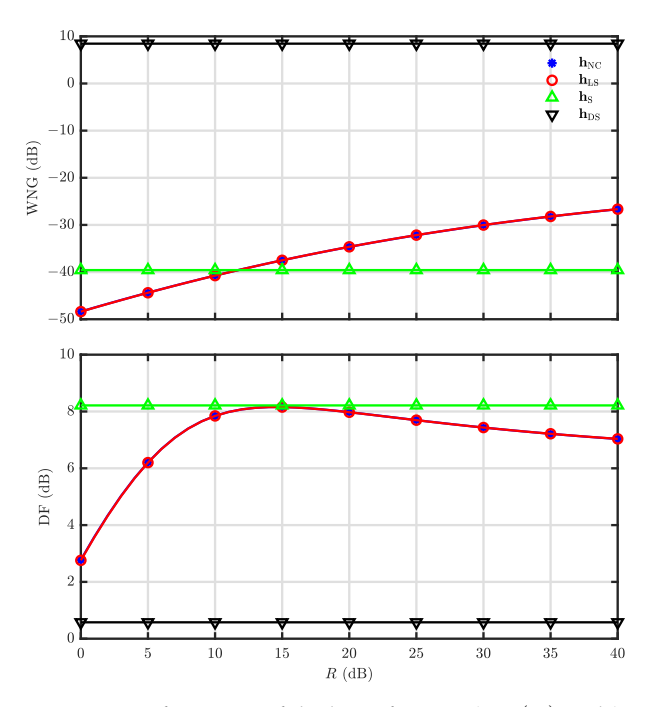


Figure 9. Performance of the beamformers $\mathbf{h}_{NC}(\omega)$ and $\mathbf{h}_{LS}(\omega)$ versus the parameter R: WNG (top), and DF (bottom). Conditions: N=3, M=7, f=1000 Hz, r=0.02 m, and $\theta_s=0$.

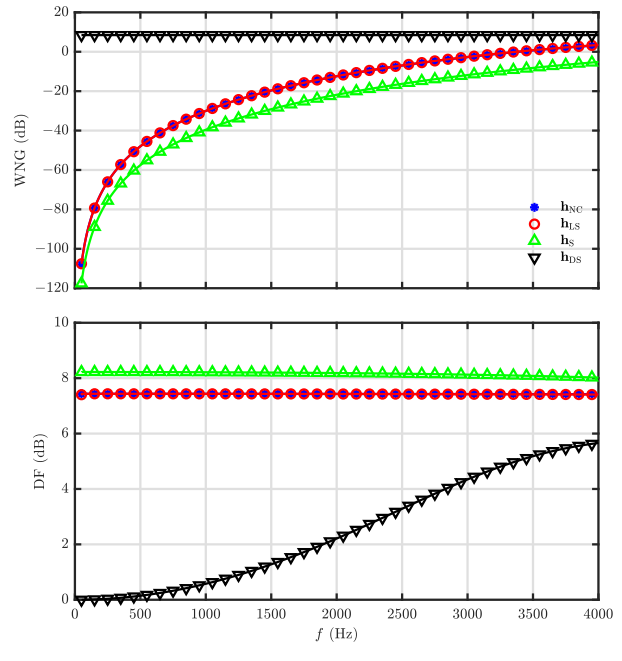


Figure 10. Performance of the beamformers $\mathbf{h}_{NC}(\omega)$ and $\mathbf{h}_{LS}(\omega)$ versus frequency: WNG (**top**), and DF (**bottom**). Conditions: N=3, M=7, R=30, r=0.02 m, and $\theta_{S}=0$.

5.3. Performance of the Minimum Norm and Combined Solutions

This simulation is devoted to the investigation of the minimum norm solution of the DMA. The desired beampattern is with N=3 and R=30. The WNG and DF versus frequency for different microphone numbers, M=7 (i.e., the null constrained solution), 10, 14, are plotted in Figure 11. Note that the inter-element spacing (which is $\delta=2r\sin\left(\frac{\pi}{M}\right)$ for a UCA, and r denotes the radius. When r=0.02 m and M=7, $\delta=0.0174$ m) keeps the same for different microphone number. From Figure 11, it is observed that the WNG increases with the microphone number, which exactly corresponds to the analysis. Figure 12 plots the beampatterns of the minimum norm beamformer with M=10 at different frequencies (f=500,1000,2000 and 4000 Hz). Comparing with the desired beampattern in Figure 2d, we observe that, though the WNG is improved at low-frequency bands, the beampattern deviates from the target at high-frequency bands also as the beamformers $\mathbf{h}_{\rm NC}(\omega)$ and $\mathbf{h}_{\rm LS}(\omega)$. For overcoming this drawback, the combined solution is derived.

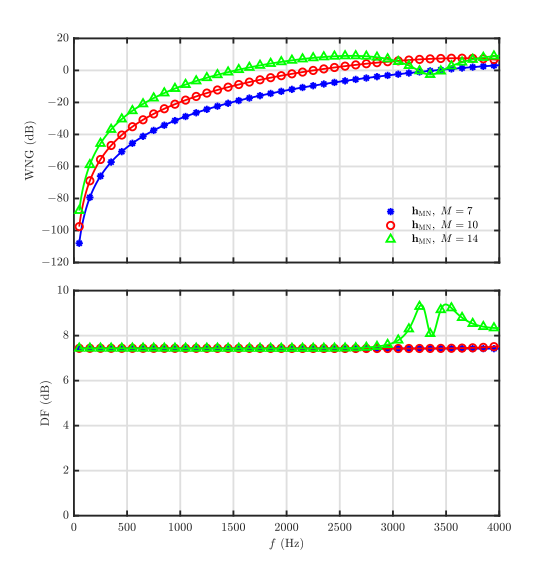


Figure 11. Performance of the beamformer $\mathbf{h}_{MN}(\omega)$ versus frequency with different microphone number, M: WNG (top), and DF (bottom). Conditions: N = 3, R = 30, $\delta = 0.0174$ m, and $\theta_{\rm S} = 0$.

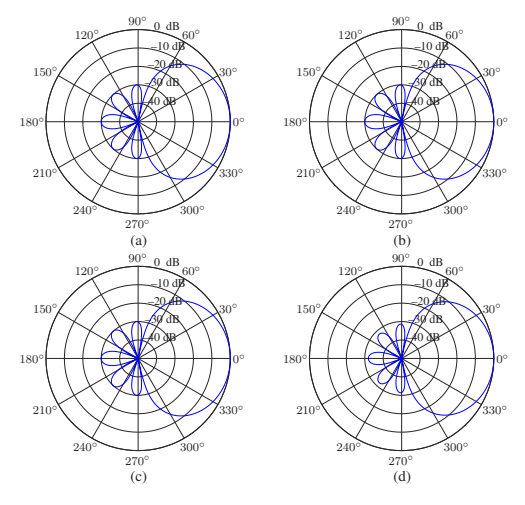


Figure 12. Beampatterns of the beamformer $\mathbf{h}_{\mathrm{MN}}(\omega)$ with different frequencies: (a) f=500 Hz, (b) f=1000 Hz, (c) f=2000 Hz, and (d) f=4000 Hz. Conditions: N=3, M=10, R=30, $\delta=0.0174$ m, and $\theta_{\mathrm{S}}=0$.

In this part, the combined solutions are studied. Again, the desired beampattern is with N=3 and R=30, and M is selected to be 10. At first, the beampatterns of $\mathbf{h}_{\mathbb{C}}(\omega)$

Sensors 2023, 23, 3733 20 of 24

with different values of μ ($\mu=1$, 0.99, 0.98, 0.95) are investigated at f=4000 Hz, and the results are shown in Figure 13. As seen, as μ decreases, the approximation of the array beampattern to the desired one goes better. Then, the performance of the beamformer $\mathbf{h}_{\mathrm{CF}}(\omega)$ with $\mu=0.2$, 0.4, 0.8, 0.9 is investigated. The WNG and DF versus frequency are plotted in Figure 14, including the results of the DS and least square ($\mu=0$) beamformers. As expected, the WNG increases and the DF decreases with the increase of μ . Figure 15 plots the 3-D beampattern of the beamformer $\mathbf{h}_{\mathrm{CF}}(\omega)$ versus the frequency with $\mu=0.4$ and $\theta_{\mathrm{S}}=0$. we can make compromises among the WNG, DF and beampattern distortion by adjusting the parameter μ flexibly. As seen from Figure 15, the level of different sidelobe keeps the same at relatively high frequencies, and we can make compromises among the WNG, DF and beampattern distortion by adjusting the parameter μ flexibly.

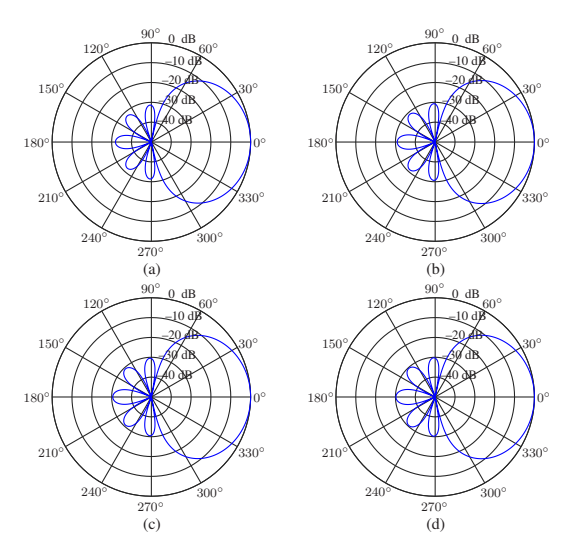


Figure 13. Beampatterns of the beamformer $\mathbf{h}_{C}(\omega)$ with different values of μ : (a) $\mu=1.0$, (b) $\mu=0.99$, (c) $\mu=0.98$, and (d) $\mu=0.95$. Conditions: N=3, M=10, R=30, $\delta=0.0174$ m, f=1000 Hz, and $\theta_{s}=0$.

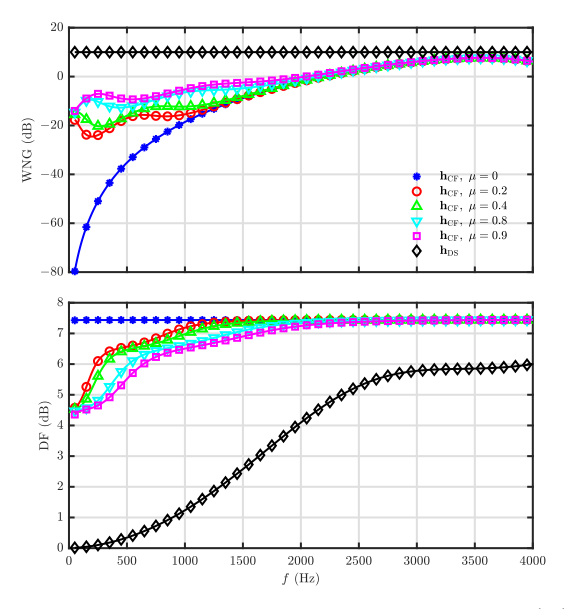


Figure 14. Performance of the beamformer $\mathbf{h}_{\mathrm{CF}}(\omega)$ versus frequency with different values of the parameter μ : WNG (**top**), and DF (**bottom**). Conditions: N=3, M=10, R=30, $\delta=0.0174$ m, and $\theta_{\mathrm{s}}=0$.

Sensors **2023**, 23, 3733 21 of 24

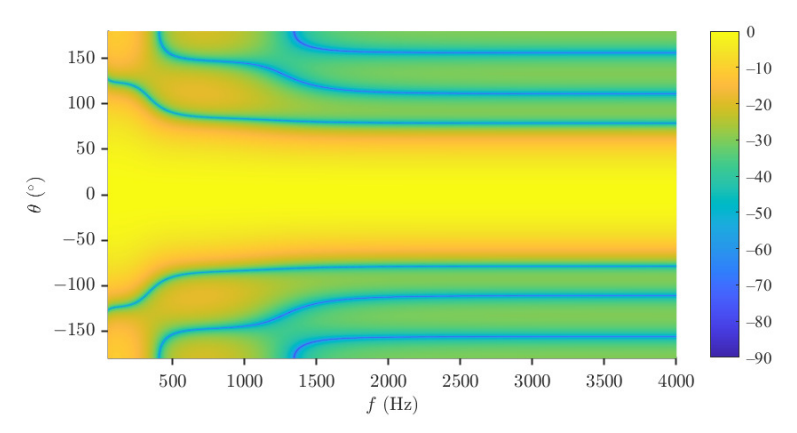


Figure 15. Beampattern of the beamformer $\mathbf{h}_{\mathrm{CF}}(\omega)$ versus frequency. Conditions: N=3, M=10, R=30, $\mu=0.4$, $\delta=0.0174$ m, and $\theta_{\mathrm{S}}=0$.

At last, we evaluate the performance of the beamformer $\mathbf{h}_{CF}(\omega)$ in the simulated room acoustic environment with image model. A UCA with radius r=0.039 m and 14 microphones, whose center and first microphone are, respectively, at (2, 2, 1.5) and (2.039, 2, 1.5), is considered in the simulation, and the loudspeaker is placed at (3.5, 2, 1.5). The reflection coefficients of all six walls are set to 0.85 and the corresponding reverberation time $T_{60}\approx 350$ ms. The simulated RIRs are divided into two parts, i.e., the direct path and reflections, based on which two metrics are defined, i.e., the direct-path-signal-to-noise ratio (DSNR), and the direct-path-signal-to-reverberation ratio (DSRR). The spatially and temporally white Gaussian noise is added to the microphone signals with DSNR = 20 dB. The input DSRR for our simulation setup is approximately 2.98 dB. The result is presented in Table 2. It can be seen that the DSNR increases and DSRR decreases with the increase of μ , which is consistent with the analysis. One should note that, the output DSNRs of the beamformer $\mathbf{h}_{CF}(\omega)$ with $\mu=0.2,\ 0.4,\ 0.8,\ 0.9$ are smaller than the input DSNR because negative WNG of the beamformer $\mathbf{h}_{CF}(\omega)$ in relatively low frequency, which can be seen in Figure 14.

Table 2. Performance of beamformer $\mathbf{h}_{CF}(\omega)$ with different value of μ . Conditions: $T_{60} \approx 350$ ms, M = 14 and r = 0.039 m, the input DSNR and DSRR are, respectively, 20 dB and 2.98 dB.

Beamformer	DSNR (dB)	DSRR (dB)
$\mathbf{h}_{\mathrm{CF}}(\omega)$, $\mu = 0.2$	5.14	4.89
$\mathbf{h}_{\mathrm{CF}}(\omega)$, $\mu=0.4$	8.24	4.74
$\mathbf{h}_{\mathrm{CF}}(\omega)$, $\mu = 0.8$	14.24	4.39
$\mathbf{h}_{\mathrm{CF}}(\omega)$, $\mu = 0.9$	15.81	4.24

6. Conclusions

In this paper, by investigating the structure of the frequency-independent beampattern of a theoretical Nth-order differential beamformer and exploiting the Chebyshev polynomials, the desired beampattern design methods which can exactly control the main lobe beamwidth and sidelobe level and obtain minimum main lobe beamwidth with a given sidelobe level are proposed. The designed beam pattern can achieve a narrower main lobe beamwidth than that of the hypercardioid beampattern with the same order, and the relationship among the main lobe beamwidth, sidelobe level and polynomial order is deduced. To obtain the designed desired beampattern, the null constrained beamformer, $\mathbf{h}_{NC}(\omega)$, and least square beamformer, $\mathbf{h}_{LS}(\omega)$, are developed, which can approximate the desired beampattern very well and consequently have a frequency-invariant spatial response at relatively low frequencies. However, the beampatterns of $\mathbf{h}_{NC}(\omega)$ and $\mathbf{h}_{LS}(\omega)$ deviate from the desired one at high frequencies. In addition, the WNG of $\mathbf{h}_{NC}(\omega)$ and $\mathbf{h}_{LS}(\omega)$ is very low at low frequencies, which means serious white noise amplification.

Sensors **2023**, 23, 3733 22 of 24

So, the minimum norm solution $\mathbf{h}_{MN}(\omega)$ and combined solutions $\mathbf{h}_{C}(\omega)$ and $\mathbf{h}_{CF}(\omega)$ are proposed, which can achieve a flexible compromise among the WNG, DF and beampattern distortion by adjusting the microphone number M and the parameter μ .

Author Contributions: Conceptualization, X.W.; methodology, X.W. and M.L.; software, X.W., M.L. and Y.Z.; validation, J.W. and X.T.; formal analysis, X.W. and Y.Z.; investigation, X.W., M.L., Y.Z., J.W. and X.T.; resources, X.W., Y.Z. and J.W.; writing—original draft preparation, X.W. and M.L.; writing—review and editing, Y.Z., J.W. and X.T.; visualization, X.W. and Y.Z.; supervision, X.W. and X.T.; funding acquisition, X.W., J.W. and X.T. All authors have read and agreed to the published version of the manuscript. All authors have read and agreed to the published version of the manuscript.

Funding: This work was supported in part by the Project Supported by Natural Science Basic Research Plan in Shaanxi Province of China under Grant 2023-JC-YB-484, in part by the National Natural Science Foundation of China under Grant 62101313, in part by Science and Technology Key Project of Shaanxi Science and Technology Department, China, under Grant 2020GY091, and in part by Doctoral Scientific Research Foundation of Shaanxi University of Science and Technology, China, under Grant 2020BJ-49.

Institutional Review Board Statement: This article does not involve ethical research and does not require ethical approval.

Informed Consent Statement: Informed consent was obtained from all subjects involved in the study.

Data Availability Statement: The data presented in this study are available on request from the corresponding author.

Conflicts of Interest: The authors declare no conflict of interest.

References

- Benesty, J.; Cohen, I.; Chen, J. Fundamentals of Signal Enhancement and Array Signal Processing; Wiley-IEEE Press: Hoboken, NJ, USA, 2017.
- Buchris, Y.; Cohen, I.; Benesty, J. On the design of time-domain differential microphone arrays. Appl. Acoust. 2019, 148, 212–222.
 [CrossRef]
- 3. Hoshiba, K.; Washizaki, K.; Wakabayashi, M.; Ishiki, T.; Kumon, M.; Bando, Y.; Gabriel, D.; Nakadai, K.; Okuno, H.G. Design of UAV-embedded microphone array system for sound source localization in outdoor environments. *Sensors* **2017**, *17*, 2535. [CrossRef] [PubMed]
- 4. Zu, X.; Guo, F.; Huang, J.; Zhao, Q.; Liu, H.; Li, B.; Yuan, X. Design of an acoustic target intrusion detection system based on small-aperture microphone array. *Sensors* **2017**, *17*, 514. [CrossRef] [PubMed]
- 5. Yu, L.; Guo, Q.; Chu, N.; Wang, R. Achieving 3D beamforming by non-synchronous microphone array measurements. *Sensors* **2020**, 20, 7308. [CrossRef]
- 6. Dehghan Firoozabadi, A.; Irarrazaval, P.; Adasme, P.; Zabala-Blanco, D.; Játiva, P.P.; Azurdia-Meza, C. 3D multiple sound source localization by proposed T-shaped circular distributed microphone arrays in combination with GEVD and adaptive GCC-PHAT/ML algorithms. *Sensors* **2022**, 22, 1011. [CrossRef]
- 7. Li, C.; Chen, C.; Gu, X. Acoustic-Based Rolling Bearing Fault Diagnosis Using a Co-Prime Circular Microphone Array. *Sensors* **2023**, 23, 3050. [CrossRef]
- 8. Prieur, F.; Rindal, O.M.H.; Austeng, A. Signal coherence and image amplitude with the filtered delay multiply and sum beamformer. *IEEE Trans. Ultrason. Ferroelectr. Freq. Control.* **2018**, *65*, 1133–1140. [CrossRef]
- 9. Lianghua, Y.; Yunfei, C.; Xiuyin, Z. Multibeam Antenna Based on Butler Matrix for 3G/LTE/5G/B5G Base Station Applications. *ZTE Commun.* **2020**, *18*, 12–18.
- 10. Dong, W.; Fanggang, W.; Xiran, L.; Pu, Y.; Dajie, J. Orthogonal Time Frequency Space Modulation in Multiple-Antenna Systems. *ZTE Commun.* **2021**, *19*, 71–77.
- 11. Sun, S.; Wen, G. Optimal Design of Wireless Power Transmission Systems Using Antenna Arrays. ZTE Commun. 2022, 20, 19–27.
- 12. Doclo, S.; Moonen, M. Design of broadband beamformers robust against gain and phase errors in the microphone array characteristics. *IEEE Trans. Signal Process.* **2003**, *51*, 2511–2526. [CrossRef]
- 13. Lin, T.; Cong, J.; Zhu, Y.; Zhang, J.; Letaief, K.B. Hybrid beamforming for millimeter wave systems using the MMSE criterion. *IEEE Trans. Commun.* **2019**, *67*, 3693–3708. [CrossRef]
- 14. Wang, Y.; Wu, W.; Zhang, X.; Zheng, W. Transformed nested array designed for DOA estimation of non-circular signals: Reduced sum-difference co-array redundancy perspective. *IEEE Commun. Lett.* **2020**, 24, 1262–1265. [CrossRef]
- 15. Patra, R.K.; Dhar, A.S. A novel nested array for real-valued sources exploiting array motion. *IEEE Signal Process. Lett.* **2021**, 28, 1375–1379. [CrossRef]

Sensors **2023**, 23, 3733 23 of 24

16. Shi, J.; Hu, G.; Zhang, X.; Zhou, H. Generalized nested array: Optimization for degrees of freedom and mutual coupling. *IEEE Commun. Lett.* **2018**, 22, 1208–1211. [CrossRef]

- 17. Yan, S. Robust time-domain broadband modal beamforming for circular arrays. *IEEE Trans. Aerosp. Electron. Syst.* **2019**, 56, 1783–1794. [CrossRef]
- 18. Dougherty, R.P.; Bozak, R. Two-dimensional modal beamforming in wavenumber space for duct acoustics. In Proceedings of the 2018 AIAA/CEAS Aeroacoustics Conference, Atlanta, GA, USA, 25–29 June 2018; p. 2805.
- 19. Yadav, S.K.; George, N.V. Sparse distortionless modal beamforming for spherical microphone arrays. *IEEE Signal Process. Lett.* **2022**, *29*, 2068–2072. [CrossRef]
- 20. Koyama, S.; Furuya, K.; Wakayama, K.; Shimauchi, S.; Saruwatari, H. Analytical approach to transforming filter design for sound field recording and reproduction using circular arrays with a spherical baffle. *J. Acoust. Soc. Am.* **2016**, *139*, 1024–1036. [CrossRef]
- 21. Chen, X.; Benesty, J.; Huang, G.; Chen, J. On the robustness of the superdirective beamformer. *IEEE/ACM Trans. Audio Speech Lang. Process.* **2021**, 29, 838–849. [CrossRef]
- 22. Trucco, A. The Statistics of Superdirective Beam Patterns. IEEE Trans. Signal Process. 2022, 70, 1959–1975. [CrossRef]
- 23. Wang, Y.; Yang, Y.; Ma, Y.; He, Z. Robust high-order superdirectivity of circular sensor arrays. *J. Acoust. Soc. Am.* **2014**, 136, 1712–1724. [CrossRef] [PubMed]
- 24. Itzhak, G.; Benesty, J.; Cohen, I. Multistage approach for steerable differential beamforming with rectangular arrays. *Speech Commun.* **2022**, *142*, 61–76. [CrossRef]
- 25. Cohen, I.; Benesty, J.; Chen, J. Differential Kronecker product beamforming. *IEEE/ACM Trans. Audio Speech Lang. Process.* **2019**, 27, 892–902. [CrossRef]
- 26. Huang, W.; Feng, J. Differential Beamforming for Uniform Circular Array with Directional Microphones; INTERSPEECH: Brno, Czech Republic, 2020; pp. 71–75.
- 27. Chen, J.; Benesty, J.; Pan, C. On the design and implementation of linear differential microphone arrays. *J. Acoust. Soc. Am.* **2014**, 136, 3097–3113. [CrossRef] [PubMed]
- 28. Pan, C.; Chen, J.; Benesty, J. Theoretical Analysis of Differential Microphone Array Beamforming and an Improved Solution. *IEEE Trans. Audio Speech Lang. Process.* **2015**, 23, 2093–2105. [CrossRef]
- 29. Huang, G.; Benesty, J.; Chen, J. Fundamental approaches to robust differential beamforming with high directivity factors. *IEEE/ACM Trans. Audio Speech Lang. Process.* **2022**, *30*, 3074–3088. [CrossRef]
- 30. Weinberger, J.; Olson, H.F.; Massa, F. A Uni-Directional Ribbon Microphone. J. Acoust. Soc. Am. 1933, 5, 139–147. [CrossRef]
- 31. Olson, H.F. Gradient microphones. J. Acoust. Soc. Am. 1946, 17, 192–198. [CrossRef]
- 32. Elko, G.W.; Gay, S.L.; Benesty, J. *Acoustic Signal Processing for Telecommunication*; Kluwer Academic Publishers: Boston, MA, USA, 2000.
- 33. Elko, G.W.; Meyer, J.; Benesty, J.; Sondhi, M.M.; Huang, Y. Springer Handbook of Speech Processing; Springer: Berlin, Germany, 2008.
- 34. Abhayapala, T.D.; Gupta, A. Higher order differential-integral microphone arrays. *J. Acoust. Soc. Am.* **2010**, 127, 227–233. [CrossRef]
- 35. Buck, M. Aspects of first-order differential microphone arrays in the presence of sensor imperfections. *Eur. Trans. Telecommun.* **2002**, *13*, 115–122. [CrossRef]
- 36. Ihle, M. Differential microphone arrays for spectral subtraction. In Proceedings of the International Workshop on Acoustic Echo and Noise Control (IWAENC), Kyoto, Japan, 8–11 September 2003; pp. 259–262.
- 37. De Sena, E.; Hacihabiboglu, H.; Cvetkovic, Z. On the design and implementation of higher order differential microphones. *IEEE Trans. Audio Speech Lang. Process.* **2011**, 20, 162–174. [CrossRef]
- 38. Song, H.; Liu, J. First-order differential microphone array for robust speech enhancement. In Proceedings of the 2008 International Conference on Audio, Language and Image Processing, Shanghai, China, 7–9 July 2008; pp. 1461–1466.
- 39. Elko, G.; Kubli, R.A.; Morgan, D.R.; West, J.E. Adjustable filter for differential microphones. *J. Acoust. Soc. Am.* **1995**, *98*, 1258–1258. [CrossRef]
- 40. Benesty, J.; Chen, J. Study and Design of Differential Microphone Arrays; Springer: Berlin, Germany, 2012.
- 41. Benesty, J.; Chen, J.; Pan, C. Fundamentals of Differential Beamforming; Springer: Berlin, Germany, 2016.
- 42. Borra, F.; Bernardini, A.; Antonacci, F.; Sarti, A. Efficient implementations of first-order steerable differential microphone arrays with arbitrary planar geometry. *IEEE/ACM Trans. Audio Speech Lang. Process.* **2020**, *28*, 1755–1766. [CrossRef]
- 43. Lovatello, J.; Bernardini, A.; Sarti, A. Steerable circular differential microphone arrays. In Proceedings of the 2018 26th European Signal Processing Conference (EUSIPCO), Rome, Italy, 3–7 September 2018; pp. 11–15.
- 44. Pan, C.; Chen, J.; Benesty, J.; Shi, G. On the design of target beampatterns for differential microphone arrays. *IEEE/ACM Trans. Audio Speech Lang. Process.* **2019**, 27, 1295–1307. [CrossRef]
- 45. Dolph, C.L. A current distribution for broadside arrays which optimizes the relationship between beam width and side-lobe level. *Proc. IRE* **1946**, *34*, 335–348. [CrossRef]
- 46. Riblet, H. Discussion on a current distribution for broadside arrays which optimizes the relationship between beamwidth and side-lobe level. *Proc. IRE* **1947**, *35*, 489–492.
- 47. Santhanakrishnan, T.; Rajesh, R.; others. An efficient destructive interference based on side lobe suppression method in sonar beamforming. *Adv. Military Technol.* **2021**, *16*, 107–120.

Sensors **2023**, 23, 3733 24 of 24

48. Nusenu, S.Y.; Basit, A.; Asare, E. FDA transmit beamforming synthesis using Chebyshev window function technique to counteract deceptive electronic countermeasures signals. *Prog. Electromag. Res. Lett.* **2020**, *90*, 53–60. [CrossRef]

- 49. Wang, S.; Lu, M.; Mei, J.; Cui, W. Deconvolved Beamforming Using the Chebyshev Weighting Method. *J. Marine Sci. Appl.* **2022**, 21, 228–235. [CrossRef]
- 50. Akkad, G.; Mansour, A.; ElHassan, B.; Le Roy, F.; Najem, M. Twiddle factor generation using chebyshev polynomials and hdl for frequency domain beamforming. In *Applications in Electronics Pervading Industry, Environment and Society: APPLEPIES 2018*; Springer: Berlin/Heidelberg, Germany, 2019; pp. 153–165.
- 51. Enache, F.; Deparateanu, D.; Enache, A.; Popescu, F. Sparse array antenna design based on dolph-chebyshev and genetic algorithms. In Proceedings of the 2016 8th International Conference on Electronics, Computers and Artificial Intelligence (ECAI), Ploiesti, Romania, 30 June–2 July 2016; pp. 1–4.
- 52. Saputra, Y.P.; Oktafiani, F.; Wahyu, Y.; Munir, A. Side lobe suppression for X-band array antenna using Dolph-Chebyshev power distribution. In Proceedings of the 2016 22nd Asia-Pacific Conference on Communications (APCC), Yogyakarta, Indonesia, 25–27 August 2016; pp. 86–89.
- 53. Khalaj-Amirhosseini, M.; Vecchi, G.; Pirinoli, P. Near-Chebyshev pattern for nonuniformly spaced arrays using zeros matching method. *IEEE Trans. Antennas Propag.* **2017**, *65*, 5155–5161. [CrossRef]
- 54. Trees, H.L.V. Detection, Estimation, and Modulation Theory, Part IV, Optimum Array Processing; John Wiley & Sons: Hoboken, NJ, USA, 2004.
- 55. Uzkov, A.I. An approach to the problem of optimum directive antenna design. In *Comptes Rendus (Doklady) de l'Academie des Sciences de l'URSS*; Academy of Sciences of the Soviet Union: Saint Petersburg, Russia, 1946; pp. 35–38.
- 56. Cox, H.; Zeskind, R.M.; Kooij, T. Practical supergain. IEEE Trans. Acoust. Speech Signal Process. 1986, ASSP-34, 393–398. [CrossRef]
- 57. Benesty, J.; Chen, J.; Cohen, I. Design of Circular Differential Microphone Arrays; Springer: Cham, Switzerland, 2015.
- 58. Abramowitz, M.; Stegun, I.A. *Handbook of Mathematical Functions with Formulas, Graphs, and Mathematical Tables*; US Government Printing Office: Washington, DC, USA, 1964; Volume 55.
- 59. Huang, G.; Benesty, J.; Chen, J. On the design of frequency-invariant beampatterns with uniform circular microphone arrays. *IEEE/ACM Trans. Audio Speech Lang. Process.* **2017**, 25, 1140–1153. [CrossRef]
- Byun, J.; Park, Y.C.; Park, S.W. Continuously steerable second-order differential microphone arrays. J. Acoust. Soc. Am. 2018, 143, EL225–EL230. [CrossRef]
- 61. Leng, X.; Chen, J.; Benesty, J. A New Method to Design Steerable First-Order Differential Beamformers. *IEEE Signal Process. Lett.* **2021**, *28*, 563–567. [CrossRef]
- 62. Jin, J.; Huang, G.; Wang, X.; Chen, J.; Benesty, J.; Cohen, I. Steering study of linear differential microphone arrays. *IEEE/ACM Trans. Audio Speech Lang. Process.* **2020**, *29*, 158–170. [CrossRef]
- 63. Wang, X.; Benesty, J.; Cohen, I.; Chen, J. Microphone array beamforming based on maximization of the front-to-Back ratio. *J. Acoust. Soc. Am.* **2018**, *144*, 3450–3464. [CrossRef]
- 64. Allen, J.B.; Berkley, D.A. Image method for efficiently simulating small-Room acoustics. *J. Acoust. Soc. Am.* **1979**, *65*, 943–950. [CrossRef]
- 65. Lehmanna, E.A.; Johansson, A.M. Prediction of energy decay in room impulse responses simulated with an image-Source model. *J. Acoust. Soc. Am.* **2008**, 124, 269–277. [CrossRef]

Disclaimer/Publisher's Note: The statements, opinions and data contained in all publications are solely those of the individual author(s) and contributor(s) and not of MDPI and/or the editor(s). MDPI and/or the editor(s) disclaim responsibility for any injury to people or property resulting from any ideas, methods, instructions or products referred to in the content.